Understanding functional dynamics and conformational stability of beta-glycosidases

Ben Bdira, F.

CHAPTER 3

Stabilization of Glucocerebrosidase by Active Site Occupancy

Abstract

Glucocerebrosidase (GBA) is a lysosomal β-glucosidase that degrades glucosylceramide. Its deficiency results in Gaucher disease (GD). The effects of active site occupancy of GBA on its structural stability were examined. For this, cyclophellitol-derived activity-based probes (ABPs) that bind irreversibly to the catalytic nucleophile (E340) were used in conjunction with the potent reversible inhibitor isofagomine, for comparaison. It is demonstrated that cyclophellitol ABPs improve the stability of GBA *in vitro*, as revealed by thermodynamic measurements (T_m increase by 21 °C), and introduce resistance to tryptic digestion. The stabilizing effect of cell-permeable cyclophellitol ABPs is also observed in intact cultured cells containing wild-type GBA, N370S GBA (labile in lysosomes), and L444P GBA (exhibits impaired ER folding): all show marked increases in lysosomal forms of GBA molecules upon exposure to ABPs. The same stabilization effect is observed for endogenous GBA in the liver of wild-type mice injected with cyclophellitol ABPs. Stabilization effects similar to those observed with ABPs were also noted at high concentrations of the reversible inhibitor isofagomine. In conclusion, evidence is provided that the increase in cellular levels of GBA by ABPs and by the reversible inhibitor is in part caused by their ability to stabilize GBA folding, which increases the resistance of GBA against breakdown by lysosomal proteases. These effects are more pronounced in the case of the amphiphilic ABPs, presumably due to their high lipophilic potential, which may promote further structural compactness of GBA through hydrophobic interactions. This study provides further rationale for the design of chaperones for GBA to ameliorate Gaucher disease.

This work was published as: Ben Bdira, F., et al., Stabilization of Glucocerebrosidase by Active Site Occupancy. ACS Chemical Biology, 2017. **12**(7): p. 1830-1841.
All of the cell biology studies were conducted by: Kallemeijn, W. W., Oussoren, S. V., Scheij, S., Bleijlevens, B., Florea, B. I., van Roomen, C. P. A. A., Ottenhoff, R., van Kooten, M. J. F. M., Walvoort, M. T. C., Witte, M. D., Boot, R. G. at the Department of Medical Biochemistry Academic Medical Center, University of Amsterdam, Amsterdam (The Netherlands).

Introduction

Lysosomal β-glucosidase glucocerebrosidase (GBA) cleaves glucosylceramide, an essential step in the turnover of cellular glycosphingolipids[1,2]. GBA is co-translationally translocated into the ER, where it acquires four N-linked glycans[3]. After removal of its signal peptide, the 495-amino acids polypeptide completely folds and subsequently binds to the triple helical structure in the apical region of the integral membrane protein LIMP-2 (lysosome integral membrane protein 2, encoded by the *Scarb2* gene), which contains trafficking information in its cytoplasmic tail[4,5]. Complexed to LIMP2, GBA is transported through the Golgi apparatus, where its N-linked glycans are converted into complex-type structures[6]. The GBA−LIMP2 complex is routed to late endosomes/lysosomes, where GBA dissociates as a result of local acid pH[5,7]. GBA belongs to family 30 of glycoside hydrolase clan A (www.casy.org); its structural topology displays a typical $(\alpha/\beta)_8$TIM barrel fold that forms the catalytic domain, a β-sheets domain, and an immunoglobulin-like domain. The catalytic domain contains several loops located in the proximity of the enzyme's active site[8]. These seem to adopt multiple conformations, indicating their structural flexibility and presumably reflecting their crucial role in the enzyme's conformational stability and/or its substrate turnover[9]. Inspection of the GBA crystal structure in complex with N-nonyldeoxynojirimycin (NN-DNJ) (PDB code: 2V3E) shows that the binding site of the enzyme is formed by a hydrophilic glycon binding pocket, where the sugar ring of the inhibitor is accommodated, forming multiple hydrogen bonds with its surrounding residues. Also, an aglycon binding pocket is present, formed by a narrow hydrophobic channel in which the aliphatic tail of the inhibitor forms a cluster of hydrophobic interactions with residues Leu241, Phe246, Tyr313, Leu314, and Tyr244 (**Figure 3.2d**)[10]. Deficiency of GBA results in Gaucher disease[11]. At present, more than 200 mutations in the *gba1* gene have been linked with GD, and next to truncations and splicing defects, several hundred amino acid substitutions in GBA have been shown to cause GD[12]. Substitutions in the GBA polypeptide chain distant from the catalytic site destabilized GBA's structure, decreasing its half-life in the cell. For instance, the L444P substitution in GBA causes faulty folding of most of its molecules in the ER, followed by subsequent proteasomal degradation[13]. Homozygosity for L444P GBA nearly always leads to a severe neuronopathic course of GD, albeit with great individual variability in onset and progression[11]. Premature degradation may also occur in the case of GBA molecules with mutations in the catalytic domain. In fact, many of the documented mutations in GBA lead to defective folding and reduced transport to lysosomes[14]. An exception is the N370S GBA substitution, which is the most prevalent *gba1* mutation among caucasian GD patients. This amino acid substitution is in a loop close to the catalytic pocket and was found to affect the enzyme's pH optimum and its kinetic

parameters such as affinity for substrates and inhibitors[15-19]. Notably, the intralysosomal stability of N370S GBA is also reduced[15,16,19]. The survival of wild-type GBA within lysosomes is already relatively short ($t_{1/2}$ ~ 24−36 h), at least in cultured cells, where its intralysosomal proteolytic breakdown is supposedly mediated by cysteine proteases, as suggested by inhibition studies with leupeptin[20]. The major symptoms of GD are predominantly caused by the abnormal accumulation of glucosylceramide in lysosomes of tissue macrophages[21,22]. Lysosomal accumulation of glucosylceramide induces a multisystem disorder with various symptoms such as hepatosplenomegaly, cytopenia, and bone disease[11]. Severely affected GD patients also develop neurological symptoms, and GBA abnormalities have been recognized as a risk factor for developing α-synucleinopathies[23]. Enzyme replacement therapy (i.e., chronic intravenous administration of macrophage-targeted recombinant human GBA[24]) markedly improves visceral symptomatology in GD patients, but the inability of the infused enzyme to pass the blood-brain barrier prohibits the prevention and correction of neurological manifestations[25]. An alternative treatment might be offered by so-called pharmacological chaperones that promote the folding and stability of (mutant) GBA through interacting with its catalytic site[26-29]. These, preferably brain-permeable, small compounds should promote the folding of (mutant) GBA in the endoplasmic reticulum, resulting in increased transport of GBA to the lysosome[26-29]. Additionally, pharmacological chaperones might also stabilize GBA intra-lysosomally[15]. Whether the latter is clinically beneficial is debated since pharmacological chaperones that interact with the active site of GBA will intrinsically also inhibit its enzymatic activity. Among pharmacological chaperone candidates, one of the best studied is the iminosugar isofagomine (IFG **1**). IFG **1** increased the thermal stability of GBA at neutral pH by 8.7 °C and improved the trafficking of the N370S GBA mutant, resulting in an increase of cellular GBA levels in Gaucher patient tissues, including the brain[30]. Additionally, oral administration of IFG **1** increased GBA L444P mutant activity in mice up to 5-fold[31]. Nevertheless, IFG **1** has exhibited poor performance when tested in humans, which could be due to its high hydrophilicity. Therefore, several other lipophilic derivatives have been tested and shown to have a higher affinity and chaperoning activity toward GBA mutants. For example, the GBA inhibitors N-butyldeoxynojirimycin (NB-DNJ, Miglustat) and NN-DNJ have been applied to GD cells with relative success: NN-DNJ has been used to restore protein levels of the N370S GBA variant in fibroblasts and NN-DNJ has been shown to lead to a significant increase in the protein level of several GBA mutants in cells, with a moderate enhancement in their thermal stability *in vitro*[17,32]. The crystal structures of GBA bound to IFG **1**, NB-DNJ, and NN-DNJ have provided insights into the interactions in GBA-inhibitor complexs[10,30]. However, these crystalline states did not provide a clear correlation between the induced conformational changes in GBA upon complex formation and the mechanism by which the inhibitors stabilized GBA folding in solution. Therefore, it is aimed to elucidate this mechanism using reversible and irreversible

glycomimetic ligands with different lipophilic properties *in vitro* and to verify the findings *in vivo*. Moreover, it is aimed to address the question of whether the occupancy of the binding pocket of GBA promotes its protection against proteolytic degradation in lysosomes. In the present study, first the stabilizing effects of cyclophellitol-type activity-based probes (ABPs; **Figure 3.1a**) were examined, which permanently bind to the E340 catalytic nucleophile, on pure, recombinant GBA by utilizing its double-displacement mechanism (**Figure 3.1b**). The ABPs are β-glucose-configured cyclophellitols with a spacer possessing hydrophobic green or red fluorescent BODIPY moieties (MDW933 **4** and MDW941 **5**; **Figure 3.1a**) attached to C6[33,34]. Also conduritol β-epoxide (CBE **2**) was used as a small hydrophilic covalent inhibitor that is supposed to occupy only the glycon binding pocket of GBA. By trapping GBA in its intermediate state by forming an adduct complex with the aforementioned mechanism-based inhibitors, the contribution of the different moieties to the structural stabilization of GBA through binding site occupancy was dissected. The effect of 2-deoxy-2-fluoro-β-D-glucopyranosyl-N-phenyltrifluoroacetimidate (fluoro **3**; **Figure 3.1a**)[35], which forms a transient glycosyl-enzyme intermediate (**Figure 3.1c**), on GBA was also examined. For comparison, the effect of the potent reversible competitive GBA inhibitor IFG **1**, which has an *in vitro* IC_{50} of ~30 nM at pH 5.2 and 5 nM at pH 7.0[27] was studied. The various investigations are described herein, and their implications are discussed.

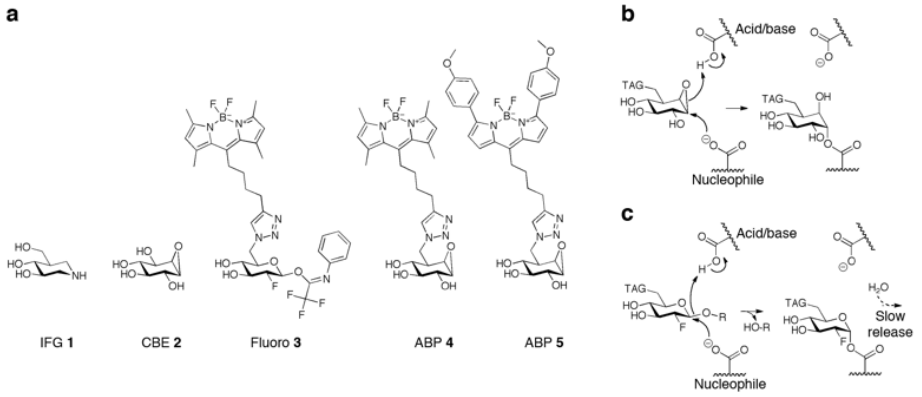

Figure 3.1. Inhibitors and reaction mechanism. (**a**) Structural formulas of competitive, reversible inhibitor isofagomine (IFG **1**), irreversible inhibitors conduritol β-epoxide (CBE **2**), semi-irreversible inhibitor-2-deoxy-2-fluoro-β-D-glucopyranosyl-N-phenyltrifluoroacetimidate[33] (fluoro**3**), cyclophellitol β-epoxide type ABP **4** (MDW933, green fluorescent), and β-epoxide-type ABP **5** (MDW941, red fluorescent)[35]. (**b**) Irreversible binding mechanism of β-epoxide-type ABPs to the nucleophile of GBA via its double-displacement mechanism. (**c**) Hydrolysis of fluoro **3** and temporary trapping of the glycosylated nucleophile adducts of GBA.

Results

Structural Stability and Flexibility of GBA: Impact of pH and Temperature

During its life cycle, GBA is exposed to a broad range of pH values: from neutral pH in the ER to an increasingly acidic pH in endosomes and lysosomes (pH 6.5 to >pH 4.5-5.0). Therefore, the effect of both acidic and neutral pH on the structural stability of purified recombinant GBA (rGBA, imiglucerase) was first investigated, by monitoring its thermal unfolding using circular dichroism. The dependence of the secondary structure of rGBA on temperature was recorded by monitoring the emission rGBA at a helical ellipticity wavelength (222 nm) while gradually heating it from 30 to 80°C (1 °C/min; see **Figure 3.2a**). The melting curve obtained for rGBA at pH 7.4 shows an apparent T_m value of 57 °C, and its melting temperature at pH 5.2 increased by 4 °C to an apparent T_m value of 61 °C. The increase in T_m at acidic pH is in agreement with previously reported measurements using differential scanning calorimetry (DSC)[15,32]. Next, the effect of neutral and acidic pH on the activity of rGBA was investigated in a time-dependent manner at 37 °C. For this purpose, rGBA was first incubated for different lengths of time at 37 °C in 150 mM McIlvaine's buffer at a pH of 5.2 or 7.4. The residual activity of rGBA was measured with the 4MU-β-D-Glc substrate in 150 mM McIlvaine buffer at pH 5.2 (**Figure 3.2b**). The data indicate that the activity of rGBA is preserved under acidic conditions, whereas at pH 7.4, its activity is lost in a time dependent manner, with a half-life of 30 min. The noted loss in rGBA activity at pH 7.4 could be due to a loss of the enzyme's native fold, apparently due to an irreversible process since the remaining activity was measured at pH 5.2. To substantiate this explanation, a limited proteolysis reaction using trypsin was performed to probe the effects of pH on the rigidity of rGBA. Here, rGBA was digested with trypsin in 150 mM McIlvaine buffer at pH 5.2 or 7.4, and the tryptic events were analyzed every 10 min by SDS-PAGE (**Figure 3.2c**). At pH 5.2, rGBA shows resistance to tryptic digestion over the course of 90 min, whereas at pH 7.4, rGBA is more sensitive to trypsin digestion, with about 40% degraded within 60 min. The activity of trypsin at pH 5.2 and 7.4 on endoglucosylceramidase (EGCII) was checked and found it to be similar (**Figure 3.3**). Of note, a tryptic fragment of approximately 34 kDa appears during proteolysis that persists over the course of the experiment, which may point to a structured and rigid domain of rGBA (**Figure 3.2c**, arrow). Mass spectrometry was used to tentatively identify the trypsin cleavage site in GBA. The results suggest that the cleavage site position could be after lysine 233 (UniProt: P04062) within the polypeptide sequence VNG**K_G**SL, located in a loop close to the active site (**Tables A2.1** and **A2.2**). In addition, this cleavage site seems to be more

accessible to trypsin digestion at neutral pH and more protected at acidic pH (**Figure 3.2d**).

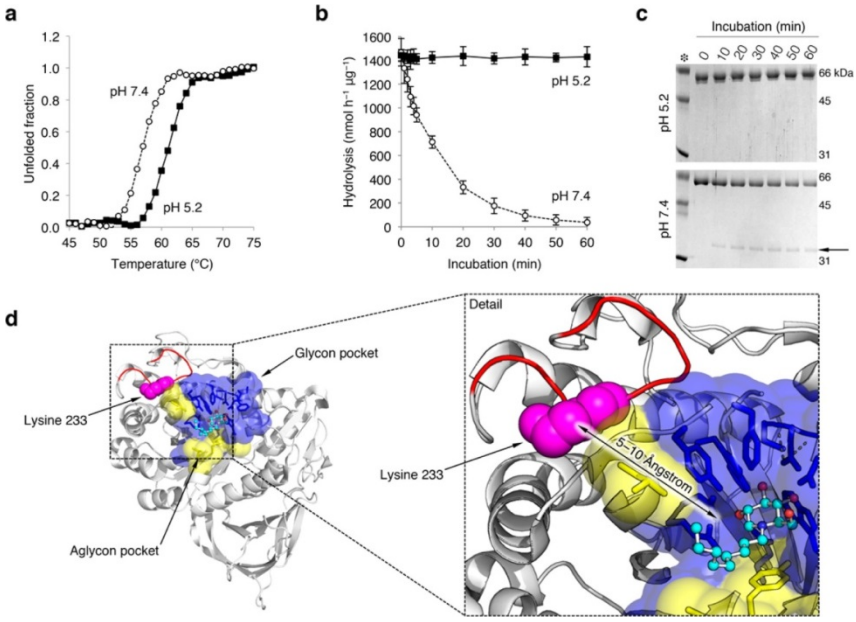

Figure 3.2. pH affects the structure of rGBA. (**a**) rGBA melting curve at pH 5.2 (closed squares) and pH 7.4 (open circles) as determined by circular dichroism. (**b**) Time-dependent decay of rGBA activity at pH 5.2 (closed squares) and pH 7.4 (open circles), as determined by hydrolysis of 4MU-β-D-Glc substrate at pH 5.2. Data are averages of duplicate values ± SD. (**c**) Coomassie brilliant blue staining of the time-dependent tryptic digestion of rGBA with a trypsin/rGBA ratio of 1/10 (w/w) at pH 5.2 and 7.4 (top and bottom, respectively). The 35 kDa tryptic fragment is highlighted by an arrow. (**d**) Trypsin cleavage site at lysine 233 (pink spheres) present on the flexible outer loop (red) shown on the crystal structure of GBA in complex with NN-DNJ (PDB code: 2V3E), with NN-DNJ shown using a ball and stick model. Amino acid residues of the glycon binding pocket of GBA are shown in blue, and residues of the aglycon site are shown in yellow. A detail view of the rendered structure is shown to the right.

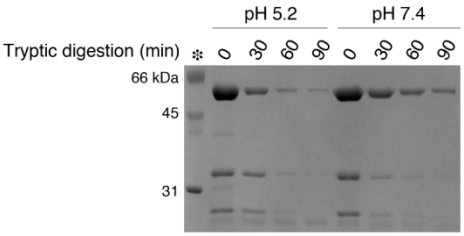

Figure 3.3. Coomassie brilliant blue staining of time-dependent, tryptic digestion of endoglycoceramidase EGCII with an optimum trypsin/EGCII ratio of 1/100 (w/w) at pH 5.2 and 7.4 (*left*, *right*, respectively).

Thermal Stability of rGBA: Impact of Glycomimetic Ligands

The effects of the competitive inhibitor IFG **1**, the semi-irreversible inhibitor fluoro **3**, and the irreversible inhibitors CBE **2** and lipophilic ABPs **4/5** on the thermal stability of rGBA were investigated at pH 5.2, mimicking lysosomal conditions. For this purpose, rGBA was incubated with saturating concentrations of inhibitors for 1 h at 37 °C and then gradually heated while monitoring tryptophan fluorescence[36,38], which decays as a result of tertiary structure unfolding. As depicted in **Figure 3.4a**, IFG **1** increased the T_m of rGBA (55.2 °C) by +5.6 °C, irreversible inhibitor **2**, by +14.1°C, 3, by +12.9 °C, and ABPs **4** and **5**, by +21.0 and +21.7 °C, respectively. Another analysis of biophysical stability was performed by circular dichroism[37]. rGBA without inhibitors was compared to the enzyme saturated with **2** and β-epoxide **4** (**Figure 3.4b**). The calculated melting temperatures of rGBA preparations follow a similar trend as that observed using tryptophan fluorescence decay. Again, β-epoxide **4** is found to exert the most prominent stabilization of rGBA.

Glycomimetic Ligands Influence the Intrinsic Fluorescence of GBA

The 12 tryptophan residues present in GBA were exploited to probe the effects of ligand binding on the general folding of GBA. Notably, Trp178 and Trp381 are in close proximity to the substrate binding pocket, and residue Trp348 (loop2) and Trp393 (loop3) reside on the protein surface; the other Trp residues are buried in the hydrophobic core of the protein[8]. rGBA emission spectra were acquired by exciting tryptophan residues at 295 nm and recording the emission by scanning from 300 to 450 nm in the presence or absence of various irreversible inhibitors (**Figure 3.3c**). In its free form, rGBA exhibits a maximum emission of 336.5 nm (similar to a previously reported value[38]). A slight 2 nm blue shift in the spectrum was observed upon complex formation with CBE **2**, with a maximum emission at 334.5 nm, reflective of a more hydrophobic environment of the tryptophan residues within the complex state (**Figure 3.3d**). rGBA exhibits a slightly larger blue shift when bound to ABPs **4** and **5**, with emission maxima of 333 nm. These data suggest that CBE **2** and ABPs **4/5** cause changes in the folding of rGBA, with the stronger effects of the latter ABPs presumably being promoted by their lipophilic tails. Serendipitously, the blue shifts induced by ABP **4** and **5** were concomitant with fluorescence quenching. As ABPs **4** and **5** contain a BODIPY fluorescence moiety (green and red fluorescent, respectively), it was speculated that part of the intrinsic GBA tryptophan emitted fluorescence is transferred to these fluorophores through an intrinsic FRET (iFRET) mechanism[39]. To test this, the fluorescence spectra of ABP **4** and ABP **5**-labeled rGBA were acquired by exciting at 295 nm and extending the scanning range to 700 nm. Indeed, two peaks appear (515 and 610 nm) at maximum emission, which represent the maximum emission for both ABP- incorporated BODIPYs (**Figure 3.3d**).

This iFRET mechanism is also supported by the overlap between the emission spectra of rGBA and ABPs (**Figure 3.5**).

Glycomimetic Ligands Variably Rigidify the Structure of GBA

Protein stabilization by ligands is generally paired with protein rigidification due to new hydrogen bonds formation or due to the formation of new clusters of hydrophobic interactions[40]. From the data presented above, it is speculated that there is a correlation between the ligand-induced conformational changes in GBA and its thermodynamic stabilization. Next it was investigated whether interactions with (ir)reversible inhibitors stabilize GBA by rigidification *in vitro*; the effect of these inhibitors on the ability of trypsin to digest rGBA was analyzed. As depicted in **Figure 3.4e,f**, only ~10% of rGBA in its free form remains after 90 min of incubation, and two major fragments are formed (~35 and ~40 kDa), which remain mostly intact over the course of the experiment. The trypsin cleavage site of the 35 kDa fragment was previously identified to be after Lys233 (**Tables A2.1** and **A2.2**). The presence of hydrophilic compounds IFG **1** or CBE **2** increased the resistance of rGBA against tryptic digestion, with 50% of rGBA remaining intact, and cleavage site of rGBA in its free state by trypsin was preserved (**Figure 3.4 e,f**). Fluoro **3** and ABPs **4** and **5** exert prominent effects on the sensitivity of rGBA to tryptic digestion (**Figure 3.4 e,f**) such that within 90 min no degradation was observed. These ABPs have long hydrophobic tails of 15-18 Å, giving them a high lipophilic potential. After binding to the nucleophile of GBA, the ABPs' hydrophobic tails further rigidify GBA through hydrophobic interactions that shield its hydrophobic core and lock into place the flexible loop that contains the trypsin cleavage site. Altogether, these observations match the incremental increases in the melting temperature of rGBA between CBE **2** and ABPs **4** and **5** (**Figure 3.4a,b**). Of note, amphiphilic inhibitors **4** and **5** also show the lowest IC_{50} values regarding the inhibition of GBA's enzymatic activity, reflecting a correlation between their stabilization effects and their high binding affinity for the catalytic pocket (**Table 3.1**).

Table 3.1. Apparent IC_{50} of Inhibitors[a]

compound	apparent IC_{50} (nM)
IFG **1**	31.4 at pH 5.2; 5.8 at pH 7.2
CBE **2**	9497 ± 42.8
fluoro **3**	5458 ± 130
ABP **4**	1.24 ± 0.04
ABP **5**	1.94 ± 0.08

[a]Values determined toward rGBA using artificial 4MUβ-D-Glc substrate, as described earlier[54].

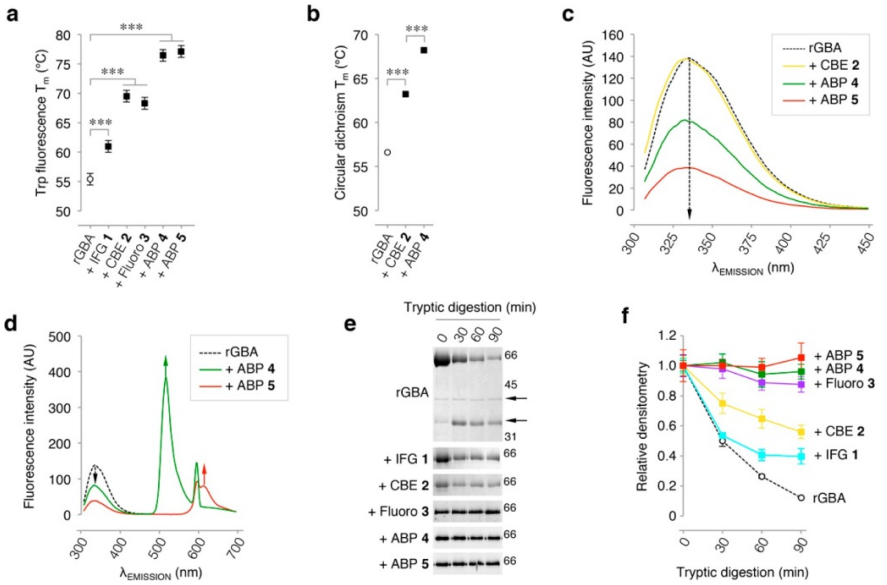

Figure 3.4. rGBA conformational changes monitored by intrinsic fluorescence and tryptic digestion. (**a**) Melting temperature (T_m) determined by tryptophan fluorescence of rGBA in the absence (control) or presence of saturating concentrations of inhibitors IFG **1**, CBE **2**, fluoro **3**, or β-epoxide ABPs **4** and 5. Statistical analysis of n = 3 experiments, two-way ANOVA (***, $p < 0.001$). (**b**) T_m determined by circular dichroism of rGBA in the absence or presence of saturating concentrations of inhibitors 2 and 4. Statistical analysis of n=2, two-way ANOVA (***, $p < 0.001$). (**c**) rGBA fluorescence spectra at λ_{EX} 295 nm in the absence of additives (black dashed line) with a maximum λ_{EM} of 335 nm, in complex with CBE **2** (yellow) with a maximum λ_{EM} of 333 nm, with ABP **4** (green) with a maximum λ_{EM} of 332 nm, and with ABP **5** (red) with a maximum λ_{EM} of 331 nm. (**d**) rGBA fluorescence spectra showing fluorescence quenching by ABP **5** (red) with the appearance of an emission peak at 610 nm and ABP **4** (green) with the emergence of an emission peak at 515 nm. All measurements were done in 10 mM phosphate buffer, 150 mM NaCl, pH 7.4. (**e**) Time-resolved analysis of the tryptic digestion of rGBA in complex with IFG 1, CBE **2**, fluoro **3**, ABP **4**, or ABP **5**. (**f**) Quantification of rGBA band densitometry during tryptic digestion in the absence (black dashed line) and presence of ABP 5 (red), ABP **4** (green), fluoro **3** (magenta), CBE **2** (yellow), or IFG **1** (cyan). Duplicate quantifications ± SD.

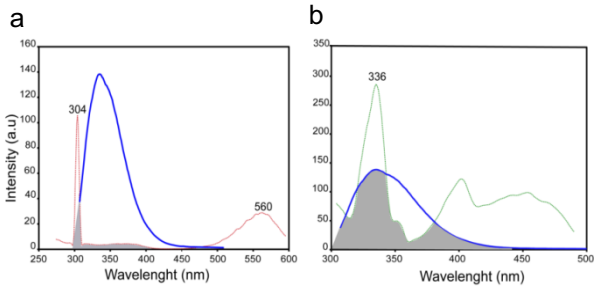

Figure 3.5: Absorption spectra of free ABPs 4 and 5 versus the emission spectrum of unlabeled rGBA. (**a**) Overlay of unlabeled rGBA emission spectrum (blue) excited at 295 nm and ABP **5** absorption spectrum (red dashed line) with a maximum absorption at 304 and 560 nm. Overlap between the spectra is highlighted in grey. (**b**) Overlay of unlabeled rGBA emission spectrum (blue) with ABP **4** absorption spectrum (green dashed line) with a maximum absorption at 336 nm. Overlap between the spectra is highlighted in grey.

Lipophilic ABPs 4 and 5 Stabilize GBA in Macrophages and Living Mice

As ABPs **4** and **5** exerted the strongest effect on the stability of rGBA *in vitro*, their influence on the enzyme *in situ* was assessed. Hence, human monocyte-derived macrophages were cultured with 100 nM ABP **5**, completely labeling all active GBA molecules (in situ IC50 ~10 nM). After a continuous pulse for up to 192 h (8 days), *in situ* ABP **5**-labeled GBA was detected by fluorescence scanning (**Figure 3.6a**). ABP **5** labeled various molecular weight forms of GBA in the range 58-66 kDa, stemming from modifications in the enzyme's N-linked glycans[41]. Earlier investigations revealed that the 58 kDa form of GBA is formed inside lysosomes as a result of N-linked glycans being trimmed by local glycsidases[41]. As seen in **Figure 3.6a**, the mature 58 kDa form of GBA accumulates when the enzyme is labeled with **5**. This finding suggests that ABP labeling stabilizes GBA against proteolytic degradation in lysosomes and does not prohibit N-glycan modifications by lysosomal glycosidases.

To further examine the stabilizing effect of ABPs on GBA *in situ*, the fate of exogenous unlabeled rGBA and the same enzyme prelabeled with ABP **4** following uptake by human monocyte-derived macrophages (**Figure 3.6b**) was analyzed. The ABP **4**-labeled enzyme was stable after uptake for at least 48 h, in sharp contrast with the rapid breakdown of unlabeled rGBA (**Figure 3.6b**). The *in situ* stabilizing effect was also visualized and verified through fluorescence microscopic analyses, showing stable ABP **4**−rGBA in monocyte-derived macrophages 48 h after uptake compared to cells loaded with rGBA (**Figure 3.6c**). Next, mice were infused intravenously with 1 nanomole of ABP **4**, which subsequently labeled endogenous GBA in various tissues[34,35,54]. In the livers of treated animals, sacrificed 6 weeks post ABP administration, **4**-labeled GBA could still be detected (**Figure 3.6d**). The amount was around ~35% of that in the livers of animals that were sacrificed 24 h after infusion of an identical dose of ABP **4** (**Figure 3.6d**, with quantification in **e**). This suggests again that ABP labeling markedly stabilizes GBA *in vivo*, since the half-life of unlabeled GBA is reported to be around 32-48 h[18,20].

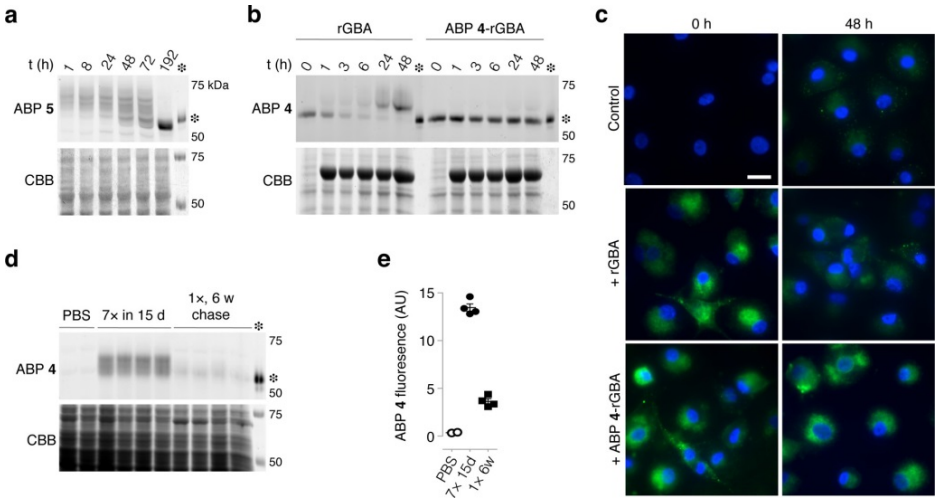

Figure 3.6. *In situ* labeling of GBA with cyclophellitol ABPs **4** and **5**. (**a**) Continuous labeling of human monocyte-derived macrophage GBA with ABP **5** (top) and Coomassie brilliant blue (CBB) staining of protein input (bottom). (**b**) Chase of ABP **4** (pre-) labeled rGBA (imiglucerase) taken up by CBE **2** pretreated human monocyte-derived macrophages (top) and CBB staining (bottom). (**c**) Fluorescence micrographs of macrophages in (**b**): control (top) and cells treated with unlabeled rGBA (middle) and ABP 4-labeled rGBA (bottom) after 0 and 48 h (left and right, respectively). Unlabeled rGBA was detected by labeling for 30 min with 10 nM ABP **4** prior to fixation. Scale bar represents 25 µm. (**d**) Chase of murine hepatic (endogenous) GBA of animals treated either with vehicle, ABP **4** for 15 days (7 injections), or a single dose 6 weeks prior to sacrifice (top) and CBB staining (bottom). (**e**) Densitometry of ABP **4**-emitted fluorescence from (d), normalized using CBB, with no treatment (open circles) or treated with repeated doses of ABP **4** (closed diamonds) or a single dose (closed squares); data are the mean of duplicate quantifications ± SEM. All gels contain 50 fmol of equimolar ABP **4**- and **5**-labeled ~59 kDa imiglucerase (asterisk) as a positive control.

Lipophilic ABPs 4 and 5 Increase GBA in Fibroblasts by Protection against Lysosomal Proteolysis

To assess whether the accumulation of ABP **4**-labeled 58 kDa GBA stems from a reduced susceptibility to lysosomal proteases, confluent human control fibroblasts were treated for 3, 5, 7, 9, or 12 days with the cysteine-cathepsin inhibitor leupeptin[18]. After harvesting the cells, GBA in the lysates of control cells and leupeptin-exposed cells was labeled with excess ABP **4** *in vitro*. As shown in **Figure 3.7a**, the amount of green fluorescent **4**-labeled GBA in untreated control cells increased slightly with culture time (top row). The incubation of the cells with Leupeptin caused a prominent accumulation of ~58 kDa active GBA over time (second row)[18]. Next, cells were incubated with red fluorescent ABP **5**. The inhibitor treatment induced a prominent time-dependent accumulation of ABP-labeled GBA (third row, **Figure 3.7a**). The increase in in situ ABP 5-labeled GBA was slightly further enhanced in cells co-incubated with leupeptin (fourth row), suggesting that **5**-labeled GBA is still prone to some degree of proteolysis within lysosomes (**Figure 3.7a**).

The quantification of ABP-labeled GBA is shown in **Figure 3.7b**, indicating that the *in situ* stabilization of GBA by leupeptin and ABP **5** at least partially overlap.

Lipophilic ABPs 4 and 5 Increase Mutant GBA Molecules in GD Fibroblasts

In fibroblasts from a homozygous N370S GBA Gaucher patient and a homozygous L444P GBA Gaucher patient, similar stabilizing effects of ABP on the enzyme were observed (**Figure 3.7c**). Both fibroblast cell lines contained a lower amount of active GBA compared to the control fibroblasts. Incubation of the cells with leupeptin and ABP **5** resulted in the stabilization of GBA, which was more prominent (6-8-fold) compared to that seen for GBA in wild- type cells (about 3-fold) (compare **Figure 3.7**, panels **b** and **d**). Exposure of both Gaucher fibroblast cell lines to the combination of ABP **5** and leupeptin further increased the stabilizing effect, which again partially overlapped (**Figure 3.7d**). Total GBA protein in cell lysates was also visualized by western blotting using the GBA-specific 8E455 antibody (**Figure 3.7e,g**, with corresponding quantification in **Figure 3.7f,h**). Again, a prominent stabilization of ~58 kDa GBA was noted with ABP **5** and/or leupeptin in the case of wild-type cells and N370S GBA Gaucher fibroblasts (**Figure 3.7**, panels **f** and **h**, respectively). Unfortunately, comparable analysis of L444P GBA Gaucher fibroblasts was not reliable due to their very low quantities of GBA protein. Overall, these findings suggest that the stabilizing effect of ABP **5** is partially caused by protection against breakdown by lysosomal proteases. This effect is specific since the lysosomal glycosidases processing GBA to its 58 kDa form do not appear to be inhibited. The reversible inhibitor IFG **1** and semi-irreversible inhibitor **3** were found to augment GBA in fibroblasts to a lesser extent. Confluent wild-type and homozygous N370S GBA fibroblasts were treated for 12 days with 0-100 μM 1. After harvesting, cell lysates were labeled with excess green ABP **4** to visualize residual active GBA molecules (**Figure 3.8a,b**). A stabilizing effect of IFG **1** became evident only at concentrations greater than 10 μM, being maximal at 100 μM (the highest concentration tested). Western blot analysis of the same experiment rendered a similar result (**Figure 3.8c,d**). The semi-irreversible inhibitor **3** comparably augmented GBA in wild-type and N370S/N370S GD fibroblasts (**Figure 3.9a,b**). The findings from treating fibroblasts with **3** were confirmed by western blot analysis (**Figure 3.9c,d**).

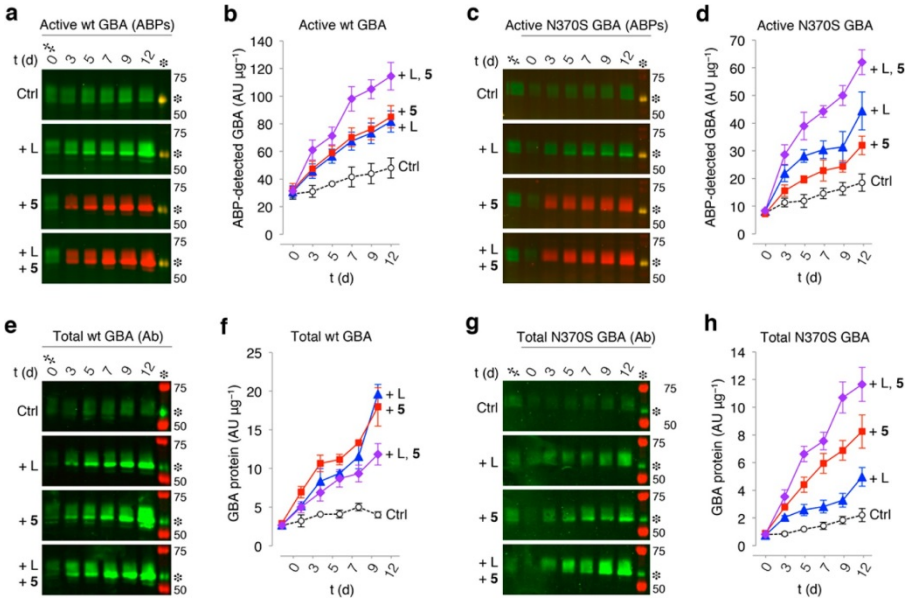

Figure 3.7. *In situ* stabilization of GBA by ABP **5** and leupeptin. Wild-type GBA fibroblasts were incubated with leupeptin, ABP **5** (red), or both for the indicated lengths of time. (**a**) GBA levels in untreated fibroblasts (top row) and cells incubated with leupeptin (second row), visualized in vitro with ABP **4** (green). Labeling of GBA in cells in situ with ABP **5** (red, third row) and in combination with leupeptin (bottom row). Equal green and red fluorescence yields a yellow overlay; fluorescence was calibrated with 50 fmol of equimolar green ABP **4**- and red ABP **5**-labeled imiglucerase present in each SDS-PAGE gel (asterisk). (**b**) Quantification of ABP-emitted fluorescence from in vitro ABP **4**-labeled controls (open black circles), cells treated with leupeptin only (blue triangles), cells treated with in situ ABP **5**-labeled GBA (red squares), and cells treated with a combination of ABP **5**-labeled GBA and leupeptin (purple diamonds). Data are the mean of n = 2 ± SD. (**c**) GBA levels in N370S/N370S fibroblasts treated in the same manner as wild-type GBA fibroblasts in panel a, vide supra. (**d**) Quantifications of ABP fluorescence in N370S/N370S fibroblasts. (**e**) Detection of total GBA protein in wild-type fibroblasts (green) by western immunoblotting of gels depicted in panel a (molecular weight ladder is in red). (**f**) Quantification of total GBA protein from in vitro ABP **4**-labeled controls (open black circles), cells treated with leupeptin only (blue triangles), cells treated with in situ ABP **5**-labeled GBA (red squares), and cells treated with a combination of ABP **5**-labeled GBA and leupeptin (purple diamonds). Data are the mean of n = 2 ± SD. (**g**) Total GBA protein in N370S/N370S fibroblasts treated in the same manner as wild-type GBA fibroblasts in panel a, vide supra. (**h**) Quantifications of ABP fluorescence in N370S/N370S fibroblasts. All data are expressed as average of n = 2 ± SD.

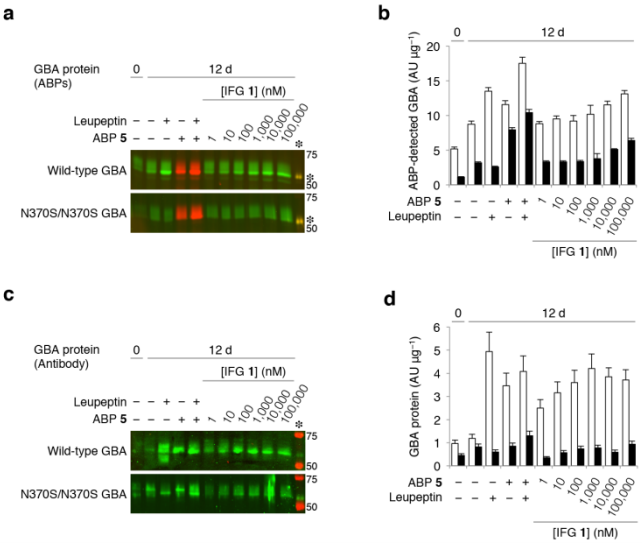

Figure 3.8: *In situ* GBA stabilization by IFG 1. Wild-type GBA (open columns) and N370S GBA (closed columns) fibroblasts were grown for 12 days in the absence or presence of incubated with leupeptin, red fluorescent ABP 5, both, or 0.001–100 µM IFG 1. (**a**) Gel depicts in situ labeling of active GBA wild type (top) and N370S variant (bottom) by ABP **5** in the presence and absence of IFG 1 and/or leupeptin. (**b**) Quantification of ABP-emitted fluorescence from *in vitro* ABP **4**-labeled controls, leupeptin and IFG 1-treated cells, compared to fluorescence of *in situ* ABP **5**-labeled GBA. (**c**) Total GBA protein in wild type (top) and N370S variant (bottom) fibroblasts lysates visualized by Western blot using GBA-specific antibody 8E4 and it densitometry quantification (d) in the presence and absence of IFG 1, leupeptin and/or ABP **5**. All data expressed as average of n = 2, ± SD.

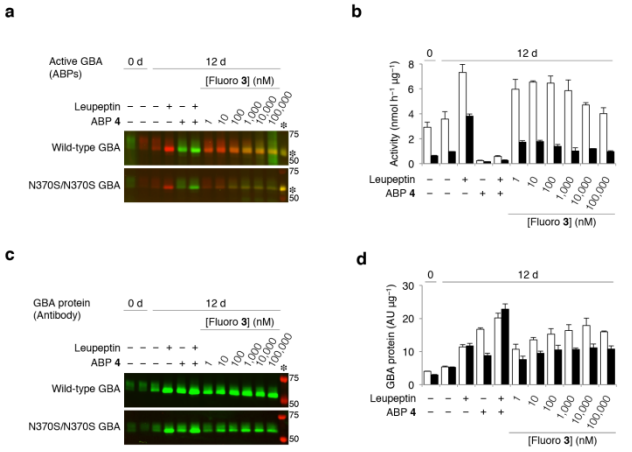

Figure 3.9: *In situ* GBA stabilization by fluoro 3. Wild-type GBA (open columns) and N370S GBA (closed columns) fibroblasts were grown for 12 days in the absence or presence of incubated with leupeptin, green fluorescent ABP **4**, both, or 0.001–100 µM fluoro **3**. (**a**) Gel depicts in situ labeling of active GBA wild type (top) and N370S variant (bottom) by ABP 4 in the presence and absence of fluoro **3** and/or leupeptin. (**b**) GBA activity towards artificial substrate in lysates shown in a. (**c**) Total GBA protein in wild type (top) and N370S variant (bottom) fibroblasts lysates visualized by Western blot using GBA-specific antibody 8E4 and it densitometry quantification (**d**) in the presence and absence of fluoro **3**, leupeptin and/or ABP **4**. All data expressed as average of n = 2, ± SD.

Discussion

In recent years, attention has been paid to the design and synthesis of chemical chaperones for GBA. Reviews by Benito et al.[28] and Jung et al.[29] cover some of the classes of glycomimetics currently under investigation as GBA chaperones. Many of these are reversible competitive, or mixed-type, inhibitors of GBA. The most well-studied chemical chaperone so far has been IFG **1**, which was the subject of several preclinical studies as well as a clinical study that did not fully meet expectations. Ambroxol[42-45], a weak, mixed-type inhibitor of GBA, has been found to augment the enzyme in cultured GD patient cells, and following oral administration to patients, an impressive reduction in spleen and liver volumes was observed. The beneficial effects of chemical chaperones on GBA in cultured cells are generally attributed to improved chaperone-assisted folding of GBA in the endoplasmic reticulum. The present investigation suggests an additional beneficial mode of action of inhibitors, i.e., the contribution of hydrophobic interactions in the GBA aglycon binding pocket to its structural stability and protection against intralysosomal proteolytic degradation.

The evidence for this notion stems from *in vitro* and *in vivo* experiments testing GBA stabilization by inhibitors. Thermodynamic measurements with pure recombinant GBA suggested that all tested inhibitors stabilized the enzyme to a degree that correlates with the strength of the inhibition. A modest stabilization of GBA was observed for small hydrophilic compounds IFG **1** and conduritol β-epoxide **2**. The lipophilic fluoro **3** and β-epoxides **4/5** equipped with hydrophobic fluorophores cause a more dramatic increase in the melting temperature of rGBA up by 21 °C. Upon complex formation with CBE **2**, GBA presents a slight shift toward the blue region of its fluorescence spectra, an indication of a conformational change, possibly resulting from orientation adjustments of its indole groups toward a more hydrophobic environment. A higher shift toward the blue region was observed when the protein was in complex with lipophilic ABPs **4** and **5**. Presumably, their lipophilic tails cause further conformational changes in which the indole groups of a tryptophan experience extra hydrophobicity. Of note, equipping cyclophellitol and cyclophellitol-aziridine with hydrophobic fluorophore tags markedly increases their affinity for GBA[33,34]. Along the same line, Vocadlo and co-workers developed an elegant fluorescence-quenched substrate for GBA by exploiting the fact that GBA accommodates the hydrophobic ceramide moiety of glucosylceramide, as it is known that GBA could tolerate a hydrophobic modification in the 6-position of glucose[46]. The designed high-affinity fluorescence-quenched substrate harbors a fluorophore attached at C6 of glucose and the hydrophobic quencher attached to the anomeric site; to a certain extent, it mimics fluoro **3** and ABPs **4** and **5**. This successful substrate design indicates again that the catalytic pocket of GBA accommodates substrates possessing a hydrophobic modification. At present, no crystal structure of GBA has been solved in the presence of the fluoro **3** or ABPs **4** and **5**. However, the crystal structure of GBA in complex with a lipophilic ligand

(NN-DNJ, PDB code: 2V3E) shows that GBA loops **1** and **2** become structured and undergo interactions with the aliphatic tails of NN-DNJ[10]. Similarly, upon complex formation with **3**, **4**, and **5**, GBA becomes extremely protected against tryptic digestion, providing strong evidence of its structural rigidification, presumably by the formation of clusters of hydrophobic interactions between the tails of the ABPs and the flexible loops in the entrance of the catalytic site of GBA. Therefore, it is presumed that the observed differences of the stabilization mechanisms between the tested compounds are mainly due to differences in their lipophilic potential. The predominant trypsin cleavage site in GBA's free state is located in a loop (residues 223-241, UniProt: P04062) close to the active site. In solution, this loop appears to be accessible for trypsin digestion by adopting a flexible conformation that fits within the protease catalytic site. Protease cleavage sites almost never occur in rigid secondary structures; they occur largely in flexible loops.[47] Interestingly, within this protein region, 16 mutations have been reported. These have been described to dramatically decrease GBA stability and activity, leading to severe GD symptoms. For instance, the L224F substitution decreases GBA activity to 4% and markedly increases its susceptibility to proteolytic degradation[48]. Mutation V230E dramatically affects GBA activity, leading to type 1 GD disease[49]. Along this line, the G232E mutation was identified in GD patients as well as patients suffering from Parkinson's disease, with the mutation markedly reducing GBA activity (~7%) and causing severe type 2 GD[50]. Moreover, substitution of G234E in GBA's sequence has severe effects on the stability and catalytic activity of the enzyme[51]. The position of the latter mutation overlaps with what it is described here as a major trypsin cleavage site. On the basis of those observations, this particular region is plausibly essential for maintaining the correct fold of GBA's catalytic domain. Upon complex formation with lipophilic ABPs, this site becomes protected against proteolytic degradation. Recently similar stabilization mechanism for another retaining β-glucosidase, endoglycoceramidase II (EGCII) from *Rhodococcus* sp[52] was noticed. The stability of EGCII was found to be improved by the formation of covalent complexes with cyclophellitols substituted with hydrophobic moieties. The tested compounds induced a more compact conformation of the flexible protein structure, revealed by an increased EGCII melting temperature, resistance against tryptic digestion, changes in its NMR spectrum, and a decrease of its exposed hydrophobic surface to the solvent, as determined by 8-anilino-1-naphthalenesulfonic acid fluorescence. Stabilization of the conformation of EGCII was correlated with the shape and hydrophobicity of the cyclophellitols substituents. The structural comparison between GBA and EGCII showed a remarkable overlap of their glycon and aglycon binding pockets[52]. Therefore, the EGCII study supports the proposed stabilization mechanism of inhibitors on the structure of GBA. Following the observed *in vitro* stabilization of GBA by inhibitors, This study was extended to living cells and mice. It is consistently noted that exposing cells (monocyte-derived macrophages and skin fibroblasts) and mice to cyclophellitol ABP **4** or **5** resulted in the

accumulation of GBA with a molecular weight of approximately 58 kDa, suggestive of lysosomal localization. Co-incubation of fibroblasts with ABPs and leupeptin, a broad lysosomal cysteine protease inhibitor known to inhibit the proteolytic breakdown of GBA, indicated that the stabilizing effect could indeed be partly ascribed to reduced lysosomal breakdown. Of note, the beneficial action of catalytic pocket occupancy by amphiphilic inhibitors on the stability and proteolytic resistance of GBA was also observed for N370S and L444P, two common mutations in GD. Clearly, irreversible covalent inhibitors **4** and **5** are of no use in the treatment of GD. However, they are valuable tools to establish the contribution of hydrophobic interactions to GBA stabilization and to selectively label the active form of GBA within living cells and laboratory animals. Fluoroglucosides, designed by Withers and co-workers[53], in theory may be more attractive as chaperones since they initially covalently bind to the catalytic nucleophile of a retaining glycosidase but are ultimately released. Therapeutic application of such compounds in patients will, however, offer the major challenge of dosing the inhibitor adequately to reach concomitant beneficial effects in all tissues: under-dosing in a tissue will be without effect and overdosing will cause undesired loss of degradative capacity in addition to GBA activity inhibition. It should also be mentioned that the natural substrate glucosylceramide may assist in the stabilization of GBA in lysosomes. In that case, intralysosomal GBA levels would be higher during high substrate flux, and the prolonged absence of substrate would promote the degradation of the enzyme. It will be of interest to examine whether a reduction of glycosphingolipids in cells by inhibition of glucosylceramide synthase activity is associated with increased lysosomal turnover of GBA.

In conclusion, GBA is significantly stabilized by the dual occupancy of its glycon and aglycon binding pockets by amphiphilic inhibitors, likely in part by promoting a global structural compactness of the enzyme associated with reduced susceptibility for proteolytic cleavage by lysosomal proteases. The findings of this study reveal new insights into the mechanism of stabilization by pharmacological chaperones that could be further exploited in the design of new compounds to rescue GBA proteostasis in GD patients.

Material and Methods

General Methods

Isofagomine **1**, fluoro **3**, and ABPs **4** and **5** were synthesized as described previously[34,35,54]. Chemicals were obtained from Sigma-Aldrich if not otherwise indicated. Recombinant GBA (rGBA, imiglucerase) was obtained from Genzyme (Cambridge, MA, USA). Gaucher patients were diagnosed on the basis of reduced GBA activity and demonstration of an abnormal genotype. Fibroblasts were obtained with consent from donors. Cell lines were cultured in Ham's F12/DMEM (Invitrogen) supplemented with 10% (v/v) FBS. Monoclonal anti-human GBA antibody 8E4 was produced from hybridoma cells as described earlier[55]. Buffy coats were purchased at Sanquin Bloodbank (Amsterdam).

Cerezyme Purification

rGBA (imiglucerase) was supplied as a sterile white lyophilized powder in the presence of mannitol and polysorbate 80 NF as stabilizer substances. Thorough purification of rGBA from its additives was conducted by affinity chromatography using a Concanavalin A-Sepharose column, eluting with a 30-min gradient of 0-1 M mannoside in 150 mM McIlvaine buffer (citric acid-Na_2HPO_4, pH 5.2). Next, an additional purification step was performed on pooled fractions using size-exclusion chromatography (Superdex 75), and elution occurred either with 150 mM McIlvaine buffer (citric acid-Na_2HPO_4, pH 5.2) or with 20 mM Tris-HCl, pH 7.4, supplemented with 150 mM NaCl. rGBA was concentrated using Amicon Ultra-4 centrifugal filter devices (30 kDa cutoff) and kept at 4 °C for further experiments.

Limited Proteolysis

Tryptic digestion of purified rGBA with or without reversible or irreversible inhibitors was performed at 37 °C either in 150 mM McIlvaine's buffer (pH 5.2 or 7.4) or in 20 mM Tris-HCl, pH 7.4, supplemented with 150 mM NaCl, using a trypsin/rGBA ratio of 1/10 (w/w) as the optimum conditions for proteolysis. Digestions were stopped with cracking buffer (50 mM Tris-HCl, pH 6.8, supplemented with 1% (w/v) SDS, 25% (v/v) glycerol, 1% (v/v) β-mercaptoethanol, and 0.05% (w/v) bromophenol blue), immediately followed by heating for 10 min at 100 °C. The tryptic digestion products (1.5-5 μg) were separated by SDS-PAGE and analyzed by Coomassie staining or, where stated, by fluorescence scanning (see below). To check the effect of acidic and neutral pH on trypsin activity, we used EGCII as a control. The same proteolysis conditions (see above) were applied with an optimum trypsin/EGCII ratio of 1/ 100 (w/w).

Tryptophan Fluorescence

rGBA (50 μM) was preincubated with 1 mM IFG **1** or fluoro **3**, 10 mM conduritol β-epoxide **2**, or 100 μM cyclophellitol ABP **4** or **5** in 150 mM McIlvaine's buffer (citric acid−Na2HPO4, pH 5.2, supplemented with 0.2% (w/v) sodium taurocholate and 0.1% (v/v) Triton X-100) for 3 h at 37 °C. Fluorescence decay curves were obtained by diluting the rGBA-inhibitor complex to 1 μM in Nanopure H_2O, followed by determination of tryptophane fluorescence (λ_{EX} 295 nm, slit width 5 nm; λ_{EM} 345 nm, slit width 5 nm) while the sample temperature was increased at a rate of 1.5 °C per minute. Sample temperature was controlled via a PTP-1 Fluorescence Peltier system (PerkinElmer). We defined the inflection point of the temperature-induced decrease in tryptophan fluorescence intensity as the melting temperature (T_m). This value was determined by taking the minimum value of the first-derivative of the slope, at which the negative slope is maximal, using GraphPad Prism 5.1. Tryptophan emission fluorescence spectra were mapped using λ_{EX} 295 nm (slit width 5 nm) and scanning emission at λ_{EM} 300−470 (slit width 5 nm; Cary Eclipse fluorescence spectrophotometer, Agilent Technologies). Samples were composed of 5 μM purified rGBA with or without **2**, **4**, or **5** in 10 mM potassium phosphate buffer (K_2HPO_4-KH_2PO_4, pH 7.4) supplemented with 150 mM NaCl. Spectral backgrounds were corrected and smoothed using Cary Eclipse fluorescence spectrophotometer software. To obtain the different protein-inhibitor complexes, purified rGBA was preincubated with inhibitors in excess for 3 h at 37 °C in 150 mM McIlvaine buffer. After labeling, excess irreversible inhibitor was removed via buffer exchange into 10 mM potassium phosphate buffer using Centriprep filter devices (30 kDa cutoff).

Circular Dichroism

Spectra were recorded on a Chirascan CD spectrometer (Applied Photophysics). Far-UV CD spectra were recorded from 180 to 300 nm in a 1 mm path length quartz cuvette (Hellma) at 20 °C at a concentration of ca. 10 μM. Spectra were collected for 0.5 s per data point at a 0.5 nm step size (spectral bandwidth was 1 nm) and were corrected for background signals. A Peltier element was used to control the sample temperature and allow the temperature to be ramped at 1 °C per minute. The intensity of the CD signal was monitored at various wavelengths (204, 215, and 235nm). The unfolding transition point (T_m) of free purified rGBA at different pH values (5.2 or 7.4) was measured by following the ellipticity signal decay at 222 nm by applying a heating rate of 1 °C per minute over a temperature gradient from 30 to 80 °C in 10 mM potassium phosphate buffer (K_2HPO_4-KH_2PO_4, pH 5.2 or 7.4), supplemented with 150 mM NaCl. The melting curves were fitted, and the T_m's were calculated using GraphPad Prism 5.1.

Enzyme Activity Assays

The residual β-glucosidase activity associated with GBA was assayed at 37 °C by incubating samples with 3.75 mM 4-methylumbelliferyl-β-D-glucopyranoside (4MU-β-D-Glc) as substrate in 150 mM McIlvaine buffer, pH 5.2, supplemented with 0.1% (w/v) BSA, 0.2% (w/v) sodium taurocholate, and 0.1% (v/v) Triton X-100.56 The half-maximal inhibitory concentrations (IC_{50}) of compounds 1-5 were measured as published previously[54]. The time-dependent decay of rGBA activity was assessed by incubating rGBA for 0-60 min at 37 °C, and at various time points, the residual rGBA activity was assessed by adding substrate. Assays were stopped with excess NaOH−glycine (pH 10.3), and fluorescence was measured with a LS30/LS55 fluorimeter (PerkinElmer) using λ_{EX} 366 nm and λ_{EM} 445 nm.

Isolation and Maturation of Macrophages.

Buffy coats were diluted into PBS supplemented with 0.1% (w/v) BSA and heparin, subsequently layered on top of a Lymphoprep gradient (Stemcell Technologies), and centrifuged at 1000g for 15 min at room temperature (RT). After washing the peripheral blood mononuclear cell pellets with PBS supplemented with 0.1% (w/v) BSA, cells were centrifuged at 750g for 10 min at RT and rinsed, and this was repeated at 500g for 5 min. Hereafter, the pellet was washed with aforementioned PBS and centrifuged at 250g for 10 min at RT. Then, monocytes were separated on a Percoll gradient. The resulting pellet was resuspended in 2.5 mL of 60% (w/v) SIP, layered with 5 mL of 45% (w/v) SIP and 2.0 mL of 34% (w/v) SIP, and centrifuged at 1750 g for 45 min at RT. The upper interface containing monocytes was washed thrice with the aforementioned PBS, centrifuged at 500g for 10 min, and then centrifuged twice at 500g for 5 min. The cell fraction was then resuspended in RPMI medium supplemented with 1% (w/v) human serum; the monocytes were counted with tryphan blue staining, and106 monocytes were seeded per well. After 1 h at 37 °C in a 5% (v/v) CO_2 atmosphere, non-adherant nonmonocyte cells were washed away with the aforementioned PBS and the adherent monocytes were cultured in RPMI medium supplemented with 10% (v/v) human serum for 7 days prior to experiment initiation.

Continuous β-Epoxide ABP *5* Pulse in Human Monocyte-Derived Macrophages

Human monocyte-derived macrophages were switched to X-VIVO 15 medium (Lonza) lacking human serum and continuously pulsed with 100 nM β-epoxide ABP 5. After 0-192 h (8 days), cells were washed extensively with PBS and lysed by scraping them in 25 mM potassium phosphate buffer (pH 6.5, supplemented with 0.1% (v/v) Triton X-100 and protease inhibitor cocktail (Roche). Protein concentrations were determined, and 10 µg of total protein (20 µL) was denatured with 5× Laemmli buffer (50% (v/v) 1 M Tris-HCl, pH 6.8, 50% (v/v) glycerol, 10% (w/v) DTT, 10% (w/v) SDS, 0.01% (w/v) bromophenol blue), boiled for 4 min at 100 °C, and separated by electrophoresis on a 7.5% (w/v) SDS-PAGE gel running continuously at 90 V.[34,35,54-56] Wet slab gels were scanned for fluorescence using a Typhoon variable mode imager (Amersham Biosciences) using λ_{EX} 488 nm and λ_{EM} 520 nm (band pass filter 40 nm) for green fluorescent fluoro ABP 3 and β-epoxide ABP **4** and λ_{EX} 532 nm and λ_{EM} 610 nM (band pass filter 30 nm) for red fluorescent β-epoxide ABP **5**. ABP-emitted fluorescence was quantified using ImageJ software (NIH, Bethesda, USA) and verified in-gel by the presence of 50 fmol of equimolar green β-epoxide ABP **4**- and red ABP **5**-labeled imiglucerase. After fluorescence scanning, SDS-PAGE gels were fixed (50/40/10 MeOH/H_2O/HAc) for 1 h, stained for total protein (50/40/10 with 1% (w/v) CBB-G250), and destained (45/45/10). Coomassie brilliant blue-stained gels were scanned on a flatbed scanner.

Determination of *in Situ* IC_{50}.

Confluent human skin control fibroblasts with wild-type GBA were incubated with 0-100 µM IFG **1**, 0-10 µM fluoro ABP **3**, or 0-100 nM β-epoxide ABP **4** for 2 h at 37 °C, and GBA-associated β-glucosidase activity was subsequently determined by incubating them in the presence or absence of 250 µM fluorescein-di-β-D-glucopyranoside (FDG) for 1 h at 37 °C. Next, cells were suspended by trypsinization, fixed in 3% (w/v) *p*-formaldehyde, and analyzed by FACS using the FL1 channel (λ_{EX} 488 nm) of a FACSCalibur (BD Biosciences). In the case of reversible inhibitor 1, all procedures, including washing with PBS, occurred in the presence of 1 at the concentration employed during the *in situ* incubation.

Pulse-Chase of Exogenous GBA

rGBA (imiglucerase, 50 µM) was incubated with(out) 100 µM ABP **4** for 1 h in 150 mM McIlvaine buffer, pH 5.2, supplemented with 0.2% (w/v) sodium taurocholate and 0.1% (v/v) Triton X-100, at 37 °C and cleaned three times over a 30 kDa cutoff filter with PBS. Mature human monocyte-derived macrophages were incubated with 300 µM **2** for 2 h; cells were the washed extensively with PBS, incubated with 100 nM rGBA (control) or **4**-labeled rGBA with for 30 min at 37 °C, and again washed extensively; the medium was then refreshed. After 0-48 h, cells were again washed extensively with PBS and lysed by scraping in 25 mM potassium phosphate buffer (pH 6.5, supplemented with 0.1% (v/v) Triton X-100 and protease inhibitor cocktail (Roche). Protein concentrations were determined in the lysates, and of the control rGBA-treated cells, 10 µg of total protein was labeled in vitro with 1µM β-epoxide ABP **4** in McIlvaine buffer, pH 5.2, and with supplements, for 1 h at 37 °C. Finally, samples were denatured, and **4**-labeled proteins were visualized by fluorescence scanning of the SDS-PAGE slab gels. ABP-emitted fluorescence was quantified using ImageJ software (NIH, Bethesda, USA), *vide supra*.

Pulse-Chase of GBA in Living Animals.

The appropriate ethics committee for animal experiments approved all experimental procedures. C57BL/6J mice were obtained from Charles River (Wilmington, MA, USA) and fed a commercially available lab diet (CRM(E), Special Diet Services, UK). Two male C57BL/6J mice were injected intravenously via the tail vein with a single dose of 100 µL of PBS, four were injected with 100 µL of PBS containing 100 pmol of ABP **4** (~2 µg kg^{-1}) 6 weeks prior to sacrifice, and four mice received the same dose every 48 h for 15 days prior to sacrifice. At the termination of the experiment, the mice were anesthetized with FFM mix (25/25/50 fentanyl citrate/midazolam/H_2O) and then perfused via the heart into the aortic root with PBS, flowing at 3.0 mL min^{-1}, using a syringe pump (Harvard apparatus, Holliston, MA, USA). The liver was collected and directly frozen in liquid nitrogen. Homogenates were made in 25 mM potassium phosphate buffer, pH 6.5, supplemented with 0.1% (v/v) Triton X-100, and ABP 4-labeled GBA in 10 µg of total protein was analyzed via SDS-PAGE. After fluorescence scanning, SDS-PAGE gels were fixed and stained with CBB, *vide supra*.

Pulse-Chase of Normal and Gaucher Patient Skin Fibroblasts

Confluent human skin fibroblasts homozygous for wild-type, N370S, or L444P GBA were cultured with medium supplemented with 100 nM ABP **5**, 100 µM leupeptin, or both components. Medium was completely refreshed every fortnight, and after 0-12 days, cells were lysed by scraping in 25 mM potassium phosphate buffer (pH 6.5, supplemented with 0.1% (v/v) Triton X-100 and protease inhibitor cocktail (Roche). After determination of the protein concentration, 10 µg of total protein was incubated with 100 nM ABP **4** (if fibroblasts were not treated by β-epoxide ABP **5** *in situ*) dissolved in 150 mM McIlvaine buffer (pH 5.2, supplemented with 0.2% (w/v) sodium taurocholate, 0.1% (v/v) Triton X-100, and protease inhibitor cocktail (Roche) for 1 h at 37 °C. Finally, samples were analyzed by SDS- PAGE on two gels: one for fluorescence scanning followed by CBB staining and one for western blotting; this was accomplished by transferring the protein in the gel to a membrane for 1 h at 12 V, followed by blocking the membrane with 2% (w/v) BSA in TBST buffer (50 mM Tris-HCl, pH 7.4, 150 mM NaCl, 0.1% (v/v) Tween-20), incubating the membrane with a 1:1000 diluted primary mouse α-human GBA monoclonal antibody (8E4, 2% (w/v) BSA in TBST), washing with TBST for 20 min (repeated 6 times), incubating with a 1:10000 diluted secondary rabbit α-mouse IRD680 antibody (Cell Signaling, 2% (w/v) BSA in TBST), subsequent washing with TBST for 20 min (repeated 6 times), and reading the signal on an Odyssey infrared scanner (LI-COR). Fluorescence emitted by either ABP-labeled proteins or antibodies was quantified using ImageJ software (NIH, Bethesda, MD, USA), *vide supra*.

In Situ Treatment with IFG 1 or Fluoro 3.

Confluent human skin fibroblasts homozygous for wild-type, N370S, or L444P GBA were incubated for 12 days with 100 nM ABP **5**, 100 µM leupeptin, or both or with 0.001-100 µM IFG **1** or fluoro **3**. Medium was completely refreshed every fortnight, and samples were treated as described earlier, *vide supra*.

References

1. Brady, R. O., Kanfer, J. N., Bradley, R. M., and Shapiro, D. (1966) Demonstration of a deficiency of glucocerebroside-cleaving enzyme in Gaucher's disease. J. Clin. Invest. 45, 1112−1115.
2. Patrick, A. D. (1965) A deficiency of glucocerebrosidase in Gaucher's disease. Biochem. J. 97, 17C−18C.
3. Berg-Fussman, A., Grace, M. E., Ioannou, Y., and Grabowski, G.A. (1993) Human acid β-glucosidase. N-glycosylation site occupancy and the effect of glycosylation on enzymatic activity. J. Biol. Chem. 268, 14861−14866.
4. Reczek, D., Schwake, M., Schröder, J., Hughes, H., Blanz, J., Jin, X., Brondyk, W., Van Patten, S., Edmunds, T., and Saftig, P. (2007) LIMP-2 is a receptor for lysosomal mannose-6-phosphate-independent targeting of beta-glucocerebrosidase. Cell 131, 770−783.
5. Zunke, F., Andresen, L., Wesseler, S., Groth, J., Arnold, P., Rothaug, M., Mazzulli, J. R., Krainc, D., Blanz, J., Saftig, P., and Schwake, M. (2016) Characterization of the complex formed by β-glucocerebrosidase and the lysosomal integral membrane protein type- 2. Proc. Natl. Acad. Sci. U. S. A. 113, 3791−3796.
6. Aerts, J. M., Schram, A. W., Strijland, A., van Weely, S., Jonsson, L. M., Tager, J. M., Sorrell, S. H., Ginns, E. I., Barranger, J. A., and Murray, G. J. (1988) Glucocerebrosidase, a lysosomal enzyme that does not undergo oligosaccharide phosphorylation. Biochim. Biophys. Acta, Gen. Subj. 964, 303−308.
7. Saftig, P., and Klumperman, J. (2009) Lysosome biogenesis and lysosomal membrane proteins: trafficking meets function. Nat. Rev. Mol. Cell Biol. 10, 623−635. Dvir, H., Harel, M., McCarthy, A. A., Toker, L., Silman, I., Futerman, A. H., and Sussman, J. L. (2003) X-ray structure of human acid-β-glucosidase, the defective enzyme in Gaucher disease. EMBO Rep. 4, 704−709.
8. Dvir, H., Harel, M., McCarthy, A. A., Toker, L., Silman, I., Futerman, A. H., and Sussman, J. L. (2003) X-ray structure of human acid-β-glucosidase, the defective enzyme in Gaucher disease. EMBO Rep. 4, 704−709.
9. Lieberman, R. L. (2011) A Guided Tour of the Structural Biology of Gaucher Disease: Acid-β-Glucosidase and Saposin C. Enzyme Res. 2011, 973231.
10. Brumshtein, B., Greenblatt, H. M., Butters, T. D., Shaaltiel, Y., Aviezer, D., Silman, I., Futerman, A. H., and Sussman, J. L. (2007) Crystal Structures of Complexes of N-Butyl- and N-Nonyl- Deoxynojirimycin Bound to Acid β-Glucosidase: Insights into the mechanism of chemical chaperone action in gaucher disease. J. Biol. Chem. 282, 29052−29058.
11. Beutler, E., and Grabowski, G. A. (2001) Glucosylceramide Lipidosis-Gaucher Disease. In The Metabolic and Molecular Bases of Inherited Diseases (Scriver, C. R., Beaudet, A., Sly, W. S., and Valle, D., Eds.) 8th ed., McGraw-Hill, New York.
12. Hruska, K. S., LaMarca, M. E., Scott, C. R., and Sidransky, E. (2008) Gaucher disease: mutation and polymorphism spectrum in the glucocerebrosidase gene (GBA). Hum. Mutat. 29, 567−583.
13. Tan, Y. L., Genereux, J. C., Pankow, S., Aerts, J. M., Yates, J. R., 3rd, and Kelly, J. W. (2014) ERdj3 Is an Endoplasmic Reticulum Degradation Factor for Mutant Glucocerebrosidase Variants Linked to Gaucher's Disease. Chem. Biol. 21, 967−976.
14. Schmitz, M., Alfalah, M., Aerts, J. M., Naim, H. Y., and Zimmer, K. P. (2005) Impaired trafficking of mutants of lysosomal glucocerebrosidase in Gaucher's disease. Int. J. Biochem. Cell Biol. 37, 2310−2320.
15. Wei, R. R., Hughes, H., Boucher, S., Bird, J. J., Guziewicz, N., Van Patten, S. M., Qiu, H., Pan, C. Q., and Edmunds, T. (2011) X-ray and Biochemical Analysis of N370S Mutant Human Acid beta-Glucosidase. J. Biol. Chem. 286, 299−308.
16. van Weely, S., van den Berg, M., Barranger, J. A., Sa Miranda, M.C., Tager, J. M., and Aerts, J. M. (1993) Role of pH in determining the cell-type-specific residual activity of glucocerebrosidase in type 1 Gaucher disease. J. Clin. Invest. 91, 1167−1175.
17. Sawkar, A. R., Cheng, W. C., Beutler, E., Wong, C. H., Balch, W. E., and Kelly, J. W. (2002) Chemical chaperones increase the cellular activity of N370S beta -glucosidase: a therapeutic strategy for Gaucher disease. Proc. Natl. Acad. Sci. U. S. A. 99, 15428−15433.
18. Grace, M. E., Graves, P. N., Smith, F. I., and Grabowski, G. A. (1990) Analyses of catalytic activity and inhibitor binding of human acid beta-glucosidase by site-directed mutagenesis. Identification of residues critical to catalysis and evidence for causality of two Ashkenazi Jewish Gaucher disease type 1 mutations. J. Biol. Chem. 265, 6827− 6835.
19. Ohashi, T., Hong, C. M., Weiler, S., Tomich, J. M., Aerts, J. M., Tager, J. M., and Barranger, J. A. (1991) Characterization of human glucocerebrosidase from different mutant alleles. J. Biol. Chem. 266,

3661−3667.
20. Jonsson, L. M., Murray, G. J., Sorrell, S. H., Strijland, A., Aerts, J. F. G. M., Ginns, E. I., Barranger, J. A., Tager, J. M., and Schram, A. W. (1987) Biosynthesis and maturation of glucocerebrosidase in Gaucher fibroblasts. Eur. J. Biochem. 164, 171−179.
21. Ferraz, M. J., Kallemeijn, W. W., Mirzaian, M., Herrera Moro, D., Marques, A., Wisse, P., Boot, R. G., Willems, L. I., Overkleeft, H. S., and Aerts, J. M. (2014) Gaucher disease and Fabry disease: new markers and insights in pathophysiology for two distinct glyco- sphingolipidoses. Biochim. Biophys. Acta, Mol. Cell Biol. Lipids 1841, 811−825.
22. Dekker, N., van Dussen, L., Hollak, C. E., Overkleeft, H., Scheij, S., Ghauharali, K., van Breemen, M. J., Ferraz, M. J., Groener, J. E., Maas, M., Wijburg, F. A., Speijer, D., Tylki-Szymanska, A., Mistry, P. K., Boot, R. G., and Aerts, J. M. (2011) Elevated plasma glucosylsphingosine in Gaucher disease: relation to phenotype, storage cell markers, and therapeutic response. Blood 118, e118−127.
23. Siebert, M., Sidransky, E., and Westbroek, W. (2014) Glucocerebrosidase is shaking up the synucleinopathies. Brain 137, 1304−1322.
24. Barton, N. W., Brady, R. O., Dambrosia, J. M., Di Bisceglie, A. M., Doppelt, S. H., Hill, S. C., Mankin, H. J., Murray, G. J., Parker, R.I., Argoff, C. E., et al. (1991) Replacement therapy for inherited enzyme deficiency macrophage-targeted glucocerebrosidase for Gaucher's disease. N. Engl. J. Med. 324, 1464−1470.
25. Desnick, R. J., and Schuchman, E. H. (2012) Enzyme replacement therapy for lysosomal diseases: lessons from 20 years of experience and remaining challenges. Annu. Rev. Genomics Hum. Genet. 13, 307−335.
26. Zechel, D. L., Boraston, A. B., Gloster, T., Boraston, C. M., Macdonald, J. M., Tilbrook, D. M., Stick, R. V., and Davies, G. J. (2003) Iminosugar glycosidase inhibitors: structural and thermody- namic dissection of the binding of isofagomine and 1-deoxynojirimycin to β-glucosidases. J. Am. Chem. Soc. 125, 14313−14323.
27. Steet, R. A., Chung, S., Wustman, B., Powe, A., Do, H., and Kornfeld, S. A. (2006) The iminosugar isofagomine increases the activity of N370S mutant acid β-glucosidase in Gaucher fibroblasts by several mechanisms. Proc. Natl. Acad. Sci. U. S. A. 103, 13813−13818.
28. Benito, J. M., García Fernańdez, J. M., and Ortiz Mellet, C. (2011) Pharmacological chaperone therapy for Gaucher disease: a patent review. Expert Opin. Ther. Pat. 21, 885−903.
29. Jung, O., Patnaik, S., Marugan, J., Sidransky, E., and Westbroek, W. (2016) Progress and potential of non-inhibitory small molecule chaperones for the treatment of Gaucher disease and its implications for Parkinson disease. Expert Rev. Proteomics 13, 471−479.
30. Lieberman, R. L., Wustman, B. A., Huertas, P., Powe, A. C., Pine, C. W., Khanna, R., Schlossmacher, M. G., Ringe, D., and Petsko, G. A. (2007) Structure of acid beta-glucosidase with pharmacological chaperone provides insight into Gaucher disease. Nat. Chem. Biol. 3, 101−107.
31. Khanna, R., Benjamin, E. R., Pellegrino, L., Schilling, A., Rigat, B. A., Soska, R., Nafar, H., Ranes, B. E., Feng, J., Lun, Y., Powe, A. C., Palling, D. J., Wustman, B. A., Schiffmann, R., Mahuran, D. J., Lockhart, D. J., and Valenzano, K. J. (2010) The pharmacological chaperone isofagomine increases the activity of the Gaucher disease L444P mutant form of β-glucosidase. FEBS J. 277, 1618−1638.
32. Abian, O., Alfonso, P., Velazquez-Campoy, A., Giraldo, P., Pocovi, M., and Sancho, J. (2011) Therapeutic Strategies for Gaucher Disease: Miglustat (NB-DNJ) as a Pharmacological Chaperone for Glucocerebrosidase and the Different Thermostability of Velaglucerase Alfa and Imiglucerase. Mol. Pharmaceutics 8, 2390−2397.
33. Walvoort, M. T., Kallemeijn, W. W., Willems, L. I., Witte, M. D., Aerts, J. M., van der Marel, G. A., Codeé, J. D., and Overkleeft, H. S. (2012) Tuning the leaving group in 2-deoxy-2-fluoroglucoside results in improved activity-based retaining β-glucosidase probes. Chem. Commun. (Cambridge, U. K.) 48, 10386−10388.
34. Li, K. Y., Jiang, J., Witte, M. D., Kallemeijn, W. W., van den Elst, H., Wong, C. S., Chander, S. D., Hoogendoorn, S., Beenakker, T. J. M., Codeé, J. D. C., van der Marel, G. A., Aerts, J. M. F. G., and Overkleeft, H. S. (2014) Synthesis of cyclophellitol, cyclophellitol aziridine and their tagged derivatives. Eur. J. Org. Chem. 2014, 6030−6043.
35. Kallemeijn, W. W., Li, K. Y., Witte, M. D., Marques, A. R., Aten, J., Scheij, S., Jiang, J., Willems, L. I., Voorn-Brouwer, T. M., van Roomen, C. P., Ottenhoff, R., Boot, R. G., van den Elst, H., Walvoort, M. T., Florea, B. I., Codeé, J. D., van der Marel, G. A., Aerts, J. M., and Overkleeft, H. S. (2012) Novel activity-based probes for broad- spectrum profiling of retaining β-exoglucosidases in situ and in vivo. Angew. Chem., Int. Ed. 51, 12529−12533.
36. Lasch, J., Bessmertnaya, L., Kozlov, L. V., and Antonov, V. K. (1976) Thermal stability of immobilized enzymes circular dichroism, fluorescence and kinetic measurements of α-chymotrypsin attached to soluble carriers. Eur. J. Biochem. 63, 591−598.
37. Mitchell, S. (1950) A photo-electric method for measuring circular dichroism. Nature 166, 434−435.

38. Qi, X., and Grabowski, G. A. (1998) Acid β-glucosidase: intrinsic fluorescence and conformational changes induced by phospholipids and saposin C. Biochemistry 37, 11544−11554.
39. Kim, J. H., Sumranjit, J., Kang, H. J., and Chung, S. J. (2014) Discovery of coumarin derivatives as fluorescence acceptors for intrinsic fluorescence resonance energy transfer of proteins. Mol. BioSyst. 10, 30−33.
40. Celej, M. S., Montich, G. G., and Fidelio, G. D. (2003) Protein stability induced by ligand binding correlates with changes in protein flexibility. Protein Sci. 12, 1496−1506.
41. Van Weely, S., Aerts, J. M. F. G., Van Leeuwen, M. B., Heikoop, J. C., Donker-Koopman, W. E., Barranger, J. A., Tager, J. M., and Schram, A. W. (1990) Function of oligosaccharide modification in glucocerebrosidase, a membrane-associated lysosomal hydrolase. Eur. J. Biochem. 191, 669−677.
42. Maegawa, G. H., Tropak, M. B., Buttner, J. D., Rigat, B. A., Fuller, M., Pandit, D., Tang, L., Kornhaber, G. J., Hamuro, Y., Clarke, J. T., and Mahuran, D. J. (2009) Identification and characterization of ambroxol as an enzyme enhancement agent for Gaucher disease. J. Biol. Chem. 284, 23502−23516.
43. Babajani, G., Tropak, M. B., Mahuran, D. J., and Kermode, A. R. (2012) Pharmacological chaperones facilitate the post-ER transport of recombinant N370S mutant β-glucocerebrosidase in plant cells: evidence that N370S is a folding mutant. Mol. Genet. Metab. 106, 323−329.
44. Zimran, A., Altarescu, G., and Elstein, D. (2013) Pilot study using ambroxol as a pharmacological chaperone in type 1 Gaucher disease. Blood Cells, Mol., Dis. 50, 134−137.
45. Bendikov-Bar, I., Maor, G., Filocamo, M., and Horowitz, M. (2013) Ambroxol as a pharmacological chaperone for mutant glucocerebrosidase. Blood Cells, Mol., Dis. 50, 141−145.
46. Yadav, A. K., Shen, D. L., Shan, X., He, X., Kermode, A. R., and Vocadlo, D. J. (2015) Fluorescence-quenched substrates for live cell imaging of human glucocerebrosidase activity. J. Am. Chem. Soc. 137, 1181−1189.
47. Fontana, A., de Laureto, P. P., Spolaore, B., Frare, E., Picotti, P., and Zambonin, M. (2004) Probing protein structure by limited proteolysis. Acta. Biochim. Polym. 51, 299−321.
48. Liou, B., Kazimierczuk, A., Zhang, M., Scott, C. R., Hegde, R. S., and Grabowski, G. A. (2006) Analyses of Variant Acid β-Glucosidases: effects of gaucher disease mutations. J. Biol. Chem. 281, 4242−4253.
49. Miočić,S., Filocamo, M., Dominissini, S., Montalvo, A. L. E., Vlahoviček, K., Deganuto, M., Mazzotti, R., Cariati, R., Bembi, B., and Pittis, M. G. (2005) Identification and functional characterization of five novel mutant alleles in 58 Italian patients with Gaucher disease type 1. Hum. Mutat. 25, 100−100.
50. Neumann, J., Bras, J., Deas, E., O'Sullivan, S. S., Parkkinen, L., Lachmann, R. H., Li, A., Holton, J., Guerreiro, R., Paudel, R., Segarane, B., Singleton, A., Lees, A., Hardy, J., Houlden, H., Revesz, T., and Wood, N. W. (2009) Glucocerebrosidase mutations in clinical and pathologically proven Parkinson's disease. Brain 132, 1783−1794.
51. Grace, M. E., Desnick, R. J., and Pastores, G. M. (1997) Identification and expression of acid beta-glucosidase mutations causing severe type 1 and neurologic type 2 Gaucher disease in non-Jewish patients. J. Clin. Invest. 99, 2530−2537.
52. Ben Bdira, F., Jiang, J., Kallemeijn, W., de Haan, A., Florea, B. I., Bleijlevens, B., Boot, R., Overkleeft, H. S., Aerts, J. M., and Ubbink, M. (2016) Hydrophobic Interactions Contribute to Conformational Stabilization of Endoglycoceramidase II by Mechanism-Based Probes. Biochemistry 55, 4823−4835.
53. Rempel, B. P., Tropak, M. B., Mahuran, D. J., and Withers, S. G. (2011) Tailoring the specificity and reactivity of a mechanism-based inactivator of glucocerebrosidase for potential therapeutic applications. Angew. Chem., Int. Ed. 50, 10381−10383.
54. Witte, M. D., Kallemeijn, W. W., Aten, J., Li, K. Y., Strijland, A., Donker-Koopman, W. E., van den Nieuwendijk, A. M., Bleijlevens, B., Kramer, G., Florea, B. I., Hooibrink, B., Hollak, C. E., Ottenhoff, R., Boot, R. G., van der Marel, G. A., Overkleeft, H. S., and Aerts, J. M. (2010) Ultrasensitive in situ visualization of active glucocerebrosidase molecules. Nat. Chem. Biol. 6, 907−913.
55. Aerts, J. M. F. G., Donker-Koopman, W. E., Murray, G. J., Barranger, J. A., Tager, J. M., and Schram, A. (1986) A procedure for the rapid purification in high yield of human glucocerebrosidase using immunoaffinity chromatography with monoclonal antibodies. Anal. Biochem. 154, 655−663.
56. Aerts, J. M. F. G., Donker-Koopman, W. E., van der Vliet, M. K., Jonsson, L. M., Ginns, E. I., Murray, G. J., Barranger, J. A., Tager, J. M., and Schram, A. W. (1985) The occurrence of two immunologically distinguishable beta-glucocerebrosidases in human spleen. Eur. J. Biochem. 150, 565−574